Nanocarrier based on halloysite and fluorescent probe for intracellular delivery of peptide nucleic acids

Marina Massaro,[a] Emanuela Licandro,[b]*, Silvia Cauteruccio,[b] Giuseppe Lazzara,[c,d] Leonarda F. Liotta,[e] Monica Notarbartolo,[a] Françisco M. Raymo,[f] Rita Sánchez-Espejo,[g] César Viseras-Iborra,[g,h] and Serena Riela[a]*

[a]Dipartimento di Scienze Biologiche, Chimiche e Farmaceutiche (STEBICEF), University of Palermo Viale delle Scienze, 90128 Palermo, Italy. E-mail: serena.riela@unipa.it

[b]Department of Chemistry, University of Milan, 20133, Milan, Italy. E-mail: emanuela.licandro@unimi.it

[c]Dipartimento di Fisica e Chimica "E. Segrè" (DiFC), University of Palermo, Viale delle Scienze, 90128 Palermo, Italy.

[d]Consorzio Interuniversitario Nazionale per la Scienza e Tecnologia dei Materiali, INSTM, I-50121 Firenze, Italy.

[e]Istituto per lo Studio dei Materiali Nanostrutturati (ISMN)-CNR, Via Ugo La Malfa 153, Palermo 90146, Italy.

[f]Laboratory for Molecular Photonics, Department of Chemistry, University of Miami,1301 Memorial Drive, Coral Gables, FL 33146-0431.

[g]Department of Pharmacy and Pharmaceutical Technology, Faculty of Pharmacy, University of Granada, Campus of Cartuja, 18071 s/n, Granada, Spain.

[h]Andalusian Institute of Earth Sciences, CSIC-UGR, Avenida de las Palmeras 4, 18100, Armilla, Granada, Spain.

Dedicated to Prof. D. Spinelli in the occasion of his 90th birthday

ABSTRACT. The development of systems able to deliver genetic material into a target site is a challenge for modern medicine. Single-stranded peptide nucleic acids have attracted attention as promising therapeutic molecules for diagnostic and gene therapy. However, their poor cell membrane permeability represents a drawback for biomedical applications. Halloysite nanotubes (HNTs) are emerging materials in drug delivery applications both for their ability to penetrate cell membranes and for enhancing the solubility of drugs in biological media. Herein, we report the first example of the use of a nanocarrier based on halloysite labelled with fluorescent switchable halochromic oxazine molecules, to deliver a single-stranded peptide nucleic acids tetramer (PNA_{ts}) into living cells. The PNA_{ts} is covalently attached to halloysite (HNTs-PNA), whereas the fluorescent probe supramolecularly interacts with HNTs. The ability of the nanomaterial to bind complementary single-stranded DNA was assessed by resonance light scattering measurements. Finally, studies of cellular uptake were carried out by confocal laser scanning microscopy on normal and tumoral cell lines. This work highlights the usefulness of the covalent approach to generate HNTs-PNA nanomaterials for the potential targeting of future specific nucleic acids in living cells, which could open the doorway to novel possibilities for theranostic and gene therapy applications.

KEYWORDS. Halloysite nanotubes, PNA, covalent modifications, halochromic switch, cellular uptake.

INTRODUCTION. The delivery of nucleic acids into a target site has attracted considerable attention since it could be an efficient strategy for the treatment of pathologies in which the expression of specific proteins is a consequence of genetic disorders.

Among the different molecules usually employed for gene therapy, single-stranded peptide nucleic acids (PNA) have been recently reported to be of great interest.[1]

PNA are synthetic single-stranded DNA/RNA mimics known for many years and introduced by Nielsen in 1991.[2] Their chemical structure is quite different from that of natural nucleic acids, being neutral oligomers consisting of *N*-(2-aminoethyl)glycine units, that replace the sugar phosphate backbone, on which nucleobases adenine, cytosine, guanine and thymine are covalently linked through a carboxymethylene spacer. The most peculiar and notable characteristic of single-stranded PNA oligomers is the ability to recognize and to bind in a very specific manner to complementary single-stranded DNA, RNA and PNA sequences following the classical Watson-Crick base-pairing rules.[3] This property is partially a result of their neutral backbone which allows strong hybridization properties thanks to the lack of negative charge repulsion between PNA and DNA or RNA strands, as it happens instead in the case of natural nucleic acids.[3] Indeed, they can easily form PNA-DNA, PNA-RNA, and PNA-PNA duplexes or more complex structures (*e.g.* triplexes, quadruplexes, or hairpins) of higher stability and greater sequence discrimination than the corresponding DNA-DNA or DNA-RNA duplexes.[4] In addition, the non-natural polyamide backbone makes PNA resistant to enzymatic degradation by nucleases and proteases.[5] For all these reasons PNA are ideal candidates for potential applications in gene therapy and antisense diagnostics.[6-10] However, some drawbacks such as a scarce cell uptake and poor water solubility have so far greatly limited their development in the biomedical field and several strategies have been proposed to overcome these limitations. Indeed, these compounds often show poor cell membrane permeability, which significantly limits their potential clinical use.[11]

Nanostructured materials, because of their interesting physico-chemical properties, have emerged as promising tools to overcome these problems.[12] Recently, both organic and inorganic materials have been extensively studied and used as nanocarrier platforms. For example, an anti-miR221 PNA possessing octa-arginine pendants was successfully adsorbed on mesoporous silica for anticancer purposes.[13] Similarly, the same type of PNA was synthetized in the presence of porous silicon.[14]

Among the different inorganic systems which could serve as platform for biological purposes, clay minerals and in particular halloysite, possessing a tubular morphology, are emerging materials in drug

carrier and delivery applications both for their ability to penetrate cell membranes and for enhancing the solubility of drugs in biological media.[15]

Halloysite, a clay mineral belonging to the kaolin group, is an aluminosilicate with a typical hollow tubular structure (HNTs), which has shown interesting biological properties such as the ability to penetrate cellular membranes, surrounding cell nuclei.[16-18] Different studies assessed the biocompatibility of HNTs [19-21] and established that they exert relevant toxicity *in vitro* at the concentration of 1000 μg/mL;[22] whereas in *vivo* experiments highlighted that the oral administration limit is at ca. 20 mg /kg BW.[23]

Recently, it was demonstrated that the modification of HNTs external surface with suitable organic molecules allowed also the penetration of nuclear barrier and therefore HNTs could be eligible as non-viral vector for gene therapy.[20] Several studies reported the supramolecular interactions of HNTs with DNA or siRNA, showing the great potential of this clay in gene therapy.[20, 24-26] Up to now, to the best of our knowledge, no examples of covalent linkage between HNTs and single-stranded nucleic acid sequences are reported in literature. The use of HNTs in comparison to others already reported systems should be advantageous since due to their peculiar hollow tubular structure and tunable surface properties it is possible to co-delivery different species with synergistic effects.

Herein we report the first example of the use of a nanocarrier (HNTs-**8**) based on halloysite and switchable halochromic oxazine molecules (**1Cl**) to deliver a single-stranded PNA tetramer (PNA_{ts}) into living cells (Figure 1).

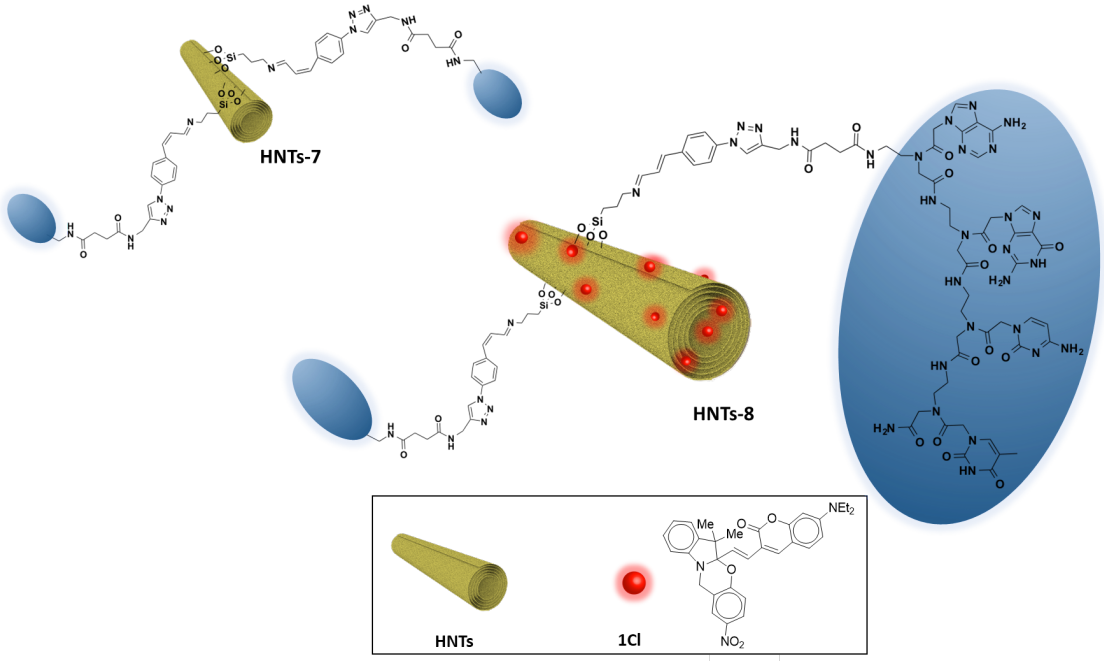

Figure 1. Schematic representation of the synthetized halloysite-PNA tetramers nanomaterial HNT-**7** and fluorescent one HNT-**8**.

The PNA_{ts} is covalently attached to halloysite surface through a pH sensitive imine bond, whereas

the fluorescent molecules supramolecularly interact with HNTs.[27] Several synthetic strategies for the linkage between HNTs derivatives and PNA_{ts} were explored, and the amount of PNA_{ts} linked onto HNTs was estimated by thermogravimetric analysis (TGA). The successful modification was verified by FT-IR and UV-*vis* spectroscopies, and differential scanning calorimetry (DSC). The morphology of obtained nanomaterial (HNTs-**7**) was studied by SEM and high angle annular dark field transmission electron microscopy (HAADF/STEM) coupled with Energy Dispersive X-ray spectroscopy (EDX). The aqueous mobility of HNTs-**7** nanomaterial was investigated by dynamic light scattering (DLS) and ζ–potential measurements. Furthermore, the ability of HNTs-**7** nanomaterial to bind complementary single-stranded DNA (ssDNA) was assessed by resonance light scattering (RLS) measurements. The capacity of HNTs to transport PNA_{ts} into cells was evaluated by confocal laser-scanning microscopy (CLSM) measurements on normal (hTERT) and tumoral cell lines (MCF-7 and HL-60R) after the labelling of HNTs-**7** with the fluorescent probe **1Cl** to obtain HNTs-**8**. Finally, to demonstrate that after internalization of the nanomaterial the PNA tetramers are still covalently linked to the clay, we evaluated the pH-sensitive nature of the covalent bond between HNTs and PNA derivatives by kinetic release experiments at different pH conditions (pH 3.0 and 7.4, respectively).

This work highlights the usefulness of the covalent approach to modify halloysite surfaces to generate HNTs-PNA nanomaterial for the potential targeting of specific nucleic acids in living cells and could open the doorway to novel possibilities for theranostic and gene therapy applications.

RESULTS AND DISCUSSION

The preparation of HNTs-**7** nanomaterial was accomplished through a click-reaction between compound **3** and modified HNT-**6**, using a convergent synthesis separately preparing: *i*) the PNA tetramer **3** endowed with an appropriate linker terminated with an alkyne group and *ii*) HNTs-**6** bearing azide moieties on the HNTs external surface (Scheme 3).

*2.1. Synthesis of PNA tetramer derivative **3***

Firstly, the resin supported PNA tetramer **1** was synthetized following a well-known procedure (see SI for details).[28] To perform the covalent linkage between the PNA_{ts} and HNTs, the resin supported PNA tetramer **1** was further modified as reported in Scheme 1. Strategy 1, based on an experimental approach reported in literature[28], was firstly investigated; however, in this case a degradation of the sequence occurred (Figure S.2).

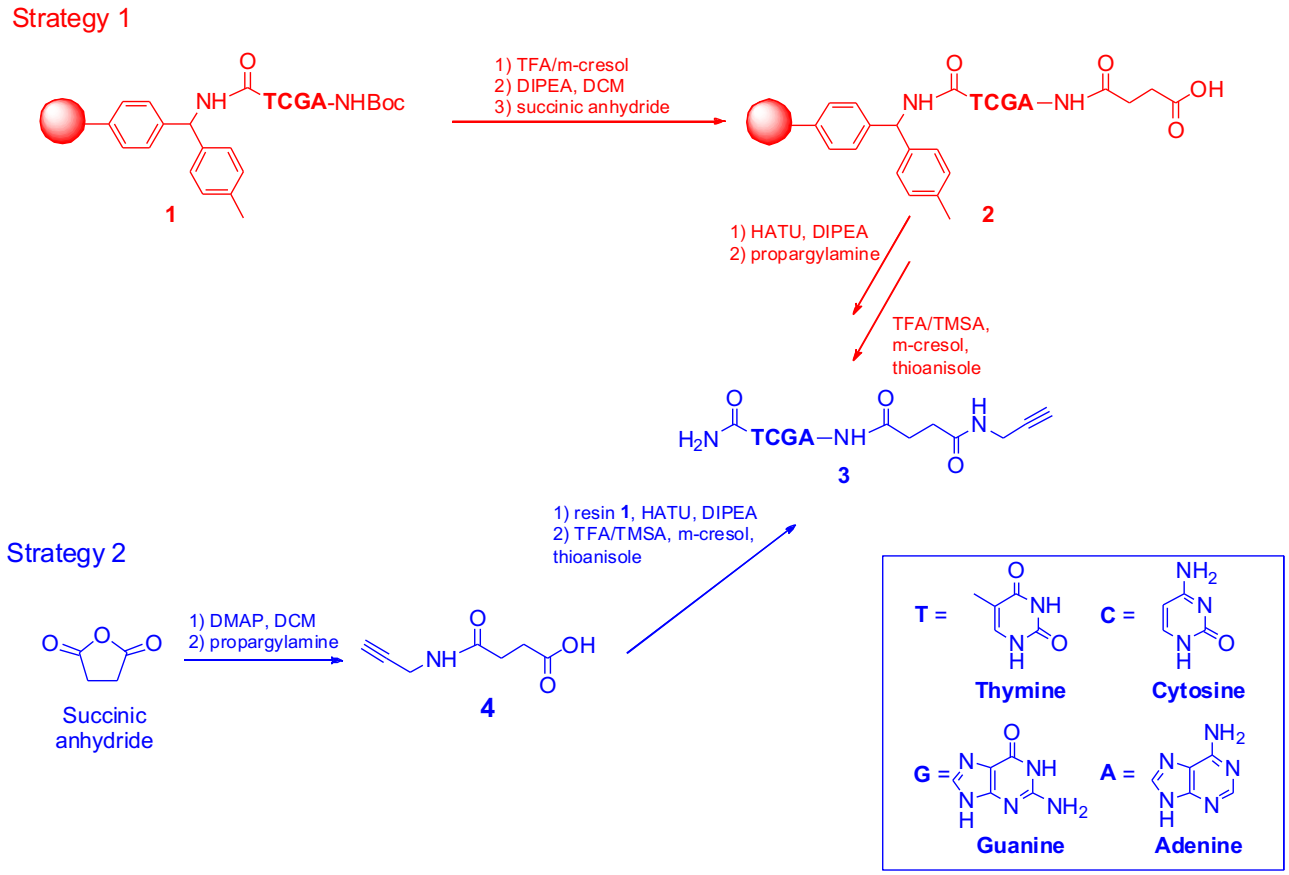

Scheme 1. Synthesis of PNA tetramer **3**.

Therefore, a different synthetic pathway was considered. In experimental strategy 2, succinic anhydride was first reacted with propargylamine, affording the intermediate **4**, which was then added to resin supported PNA **1**. The resin was subjected to cleavage by stirring it in the presence of a mixture of TFA/TFMSA/*m*-cresol/thioanisole in a 6:2:1:1 ratio for 1 h. Afterwards, the reaction mixture was filtered, and the filtrate was concentrated. To the residue so obtained Et_2O to precipitate PNA tetramer **3** as white solid. Centrifugation of the slurry gave the product, which was washed with Et_2O and dried to afford the crude tetramer, which was analyzed by RP-HPLC and ESI(+) mass analysis. As showed in Figure 2, the HPLC chromatogram showed one peak related to **3** confirming the success of the synthesis.

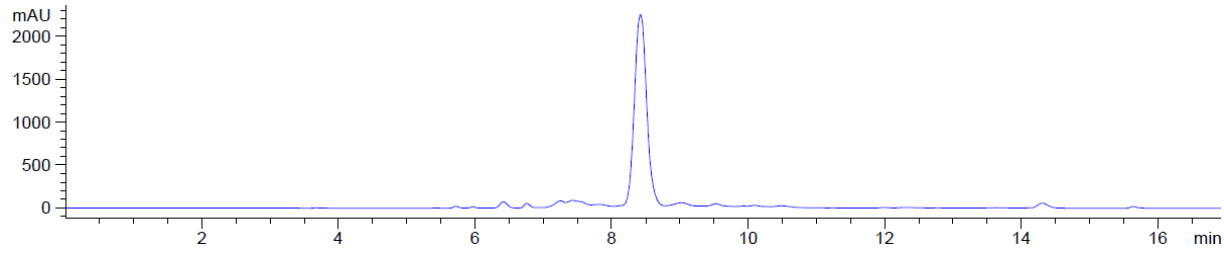

Figure 2. HPLC analysis of PNA tetramer **3** at 260.4 nm.

2.2 Synthesis of HNTs-7 nanomaterial

The HNTs-**7** nanomaterial was synthetized according to the procedure reported in Scheme 2.

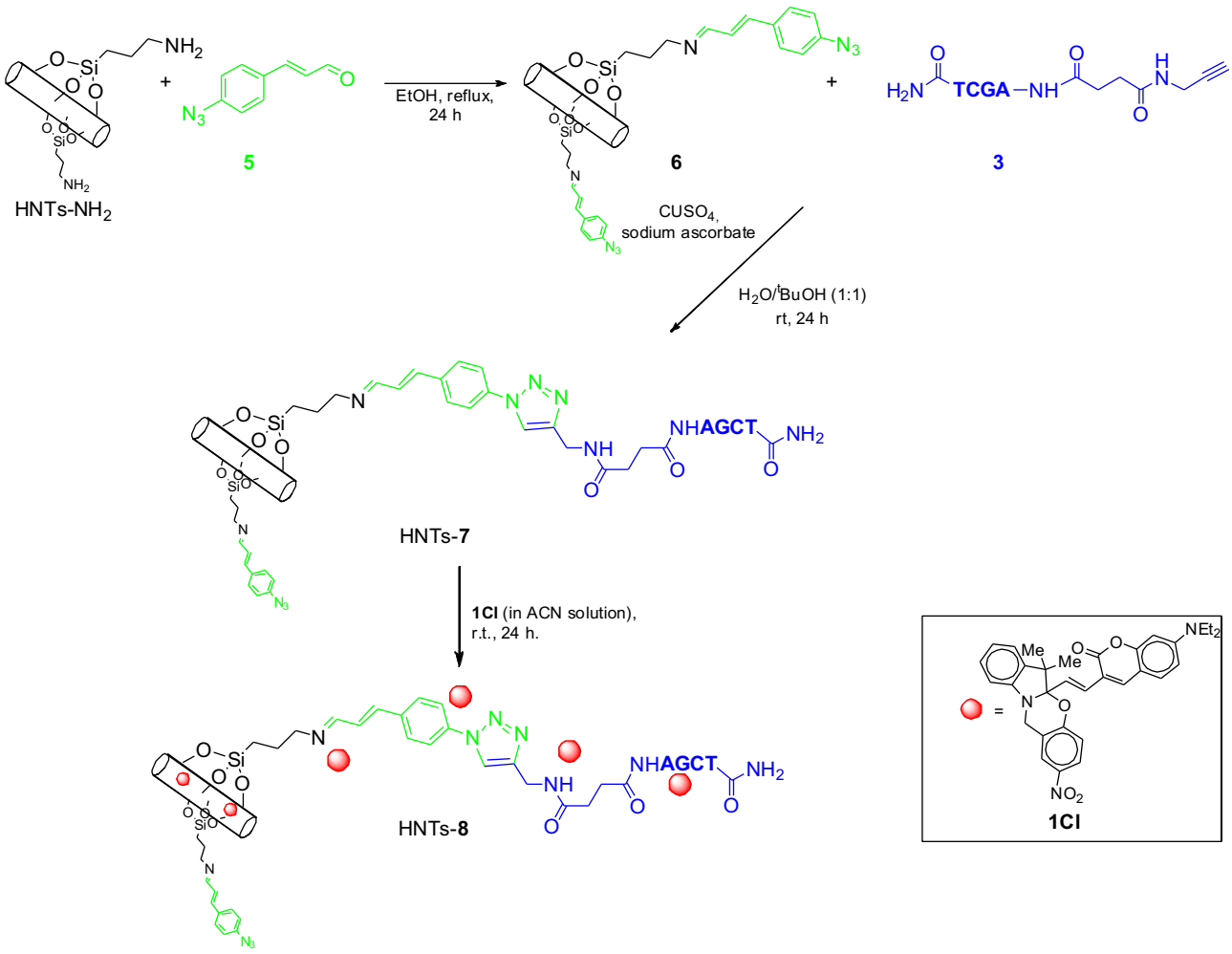

Scheme 2. Schematic representation of the synthesis of HNTs-**7** nanomaterial.

In brief, amino modified HNTs (HNTs-$\mathbf{NH_2}$)[29] (degree of functionalization of 0.63 mmol g^{-1}) was reacted with 4-azido cinnamaldehyde **5** to afford the intermediate HNT-**6** nanomaterial where the organic moiety is linked to halloysite external surface by an imine bond (Scheme 2). In a first attempt, we adopted the same experimental conditions reported in literature for the Schiff base formation on HNTs surface, using microwave irradiation as heating source (Table 1, entry 1).[30] Following this procedure (reaction time of 1 h, temperature of 78 °C and ethanol as solvent), we did not obtain any loading, as estimated by thermogravimetric analysis (TGA). Therefore, we carried out the reaction under traditional heating, by considering the effect of reaction time and temperature using ethanol as solvent. The experimental conditions and the results obtained are reported in Table 1.

Table 1. Experimental conditions for the synthesis of nanomaterial **6**.

Entry	Heating	Time (h)	T (°C)	Loading (wt%)[a]
1	MW	1	78	/

2	Trad.	4	r.t.	< 1
3	Trad.	8	r.t.	< 1
5	Trad.	24	r.t.	< 1
6	Trad.	24	78	9.5

[a]Estimated by TGA.

As it is possible to note, the best experimental conditions were obtained at a temperature of 78 °C, for a reaction time of 24 h (entry 6). In this case, we obtained a percent loading of 4-azidocinnamaldehyde on HNTs-NH_2 nanomaterial of ca. 9.5 wt% as estimated by TGA, with a degree of functionalization of 0.61 mmol g^{-1}.

Afterwards, PNA tetramer **3** was covalently linked on the HNTs-**6** nanomaterial by adopting the Meldal-Sharpless-Huisgen azide-alkyne 1,3-dipolar cycloaddition, obtaining the final nanomaterial HNTs-**7** where the PNA tetramer was linked to HNTs by a triazole ring (Scheme 2). The covalent grafting of PNA tetramer **3** was carried out at room temperature for 24 h, in the presence of $CuSO_4$ and sodium ascorbate as catalysts, in a mixture H_2O/^{t}BuOH (1:1) as solvent. Then, the obtained nanomaterial was isolated by subsequent washings with H_2O to remove the catalysts and some residual unreacted reagents.

It should be noted that in the adopted experimental conditions a partial hydrolysis of the imine bond between the cinnamaldehyde moiety and HNTs occurred as proved by the UV-*vis* analysis of the filtrate. To quantify the linker leaching during the reaction, we treated the HNTs-**6** in the same experimental conditions adopted for the click chemistry reaction but in the absence of the PNA **3** and after work-up we analyzed the obtained powder by TGA. It was found that ca. 3.2 wt% of the total amount of linker grafted was lost during the reaction (Figure S.3).

Considering these findings, we estimated a degree of functionalization of PNA tetramer onto HNTs surface of ca. 0.18 mmol g^{-1} compared to HNTs-**6** (loading of 23.5 wt%). Based on the stoichiometric ratios (0.36 mmol g^{-1} and 0.18 mmol g^{-1} for HNTs-**6** and HNTs-**7**, respectively), we determined that the mole ratio between PNA tetramer **3** and azido groups linked onto HNTs surface (HNTs-**6** nanomaterial) is 1:2. It is worth to note that complete linkage of PNA tetramer **3** on HNTs surface is not achieved probably due to steric hindrance.

Finally, the HNts-**7** nanomaterial was labelled with the fluorescent probe **1Cl** (see *infra*) to afford the fluorescent HNTs-**8** nanomaterial

The HNTs-**7** nanomaterial was thoroughly characterized by several techniques.

In Figure 3a the TGA curves recorded under air flow over the HNTs-**6** and **7** nanomaterials are displayed. According to the different chemical composition two different degradation profiles were registered for the intermediate HNT-**6** nanomaterial and the HNTs-**7**. Under air flow, the HNTs-**6**

gradually degraded from ca. 250 °C, then the weight loss progressively increased between around 300-600 °C up to stabilizing to a final mass value of 74.2 %. The HNTs-**7** is characterized by lower thermal stability in the presence of air, in comparison with the starting **6** nanomaterial and shows a pronounced weight loss between 250-500 °C in accordance with the presence of the PNA tetramer, up to reaching a stable mass value of 50.7%.

In Figure 3b are reported the FT-IR spectra of HNTs-**6** and **7**, respectively. Compared to pristine HNTs, HNTs-**6** exhibited the characteristic vibration peak of the azido groups at ca. 2100 cm^{-1} and some other vibration peaks related to the presence of the organic moieties. In detail, the peaks in the range 1600-1350 cm^{-1} related to the stretching of C=C, C=N and C–N groups, are clearly observable. After tetramer linkage, some variations in the FT-IR spectrum are observed. In particular, new bands at ca. 1583, 1508, 1440, 1414 and 1290 cm^{-1} for the stretching vibrations of the carbonyl and aromatic groups of the tetramer are present (Figure S.4). Furthermore, a decrease in the intensity of the typical stretching band of $-N_3$ groups is observed, further confirming the successful click-reaction.

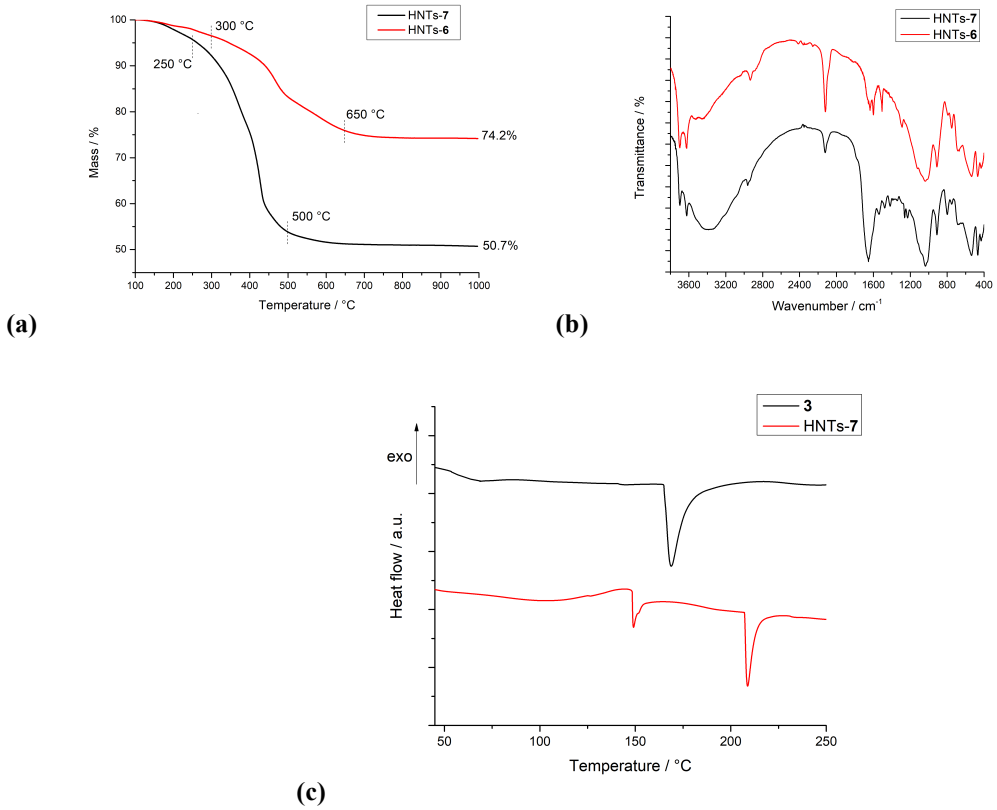

Figure 3. (a) Thermoanalytical curves and (b) FT-IR spectra of HNTs-**6** and **7** nanomaterials; (c) DSC thermograms of PNA tetramer **3** and HNTs-**7** nanomaterial.

The HNTs-**7** nanomaterial was further studied by differential scanning calorimetry (DSC). As it is possible to note from Figure 3c, the thermogram of PNA tetramer **3** reveals a melting process of at ca. 170 °C with an enthalpy change of 59.3 J g^{-1} corresponding to the melting point of the tetramer. Conversely, the HNTs-**7**, beside the typical signals related to HNTs, does not show the melting signal

for PNA, accordingly, the PNA crystallinity is lost upon HNTs interaction, further confirming the successful grafting.

Dynamic light scattering experiments have been performed in an aqueous dispersion to characterize the diffusion dynamics of HNTs-**6** and **7** nanomaterials. HNTs are anisotropic objects with a high aspect ratio, which can change with functionalization. Moreover, the particle ability to interact and aggregate can also depend on surface decoration. Thus, a detailed quantitative analysis of the results was hampered. Valuable information was achieved by using the Stokes-Einstein equation to calculate the average diameter of the equivalent sphere, which can be considered as an index to follow the changes in particle dimensions and interparticle aggregation.

A single translational diffusion mode was observed in the case of HNT-**6** dispersion with Z-average sizes (*i.e.*, the intensity weighted mean diameters) of ca. 1460 nm (greater than that of pristine HNTs) and a polydispersity index of 0.958. These findings indicated a broad size distribution of diffusing objects consistent with the presence of some aggregation phenomena in aqueous environment compatible with the presence of a hydrophobic organic moiety linked to HNTs. After the tetramer linkage, the value of the Z-average size of the nanomaterial decreased to ca. 850 nm consequently to the introduction of a more hydrophilic component onto HNTs external surface.

ζ-Potential measurements of the HNTs-**7** nanomaterial in water showed a value of -0.411 mV that indicates a reduction of surface charge upon functionalization (for a pristine HNTs ζ-potential value of -16 mV) in line with the modification of HNTs surface.

The UV–*vis* absorption spectrum of HNTs-**7** nanomaterial shows the successful linkage of PNA tetramer **3** onto HNTs. As shown in Figure 4a, the aqueous dispersion of HNTs-**7** (0.026 mg mL^{-1}) exhibited the characteristic absorption of PNA nucleobases at ca. 260 nm. It is interesting to note that, conversely to free PNA tetramer **3** (Figure S.5a), by heating the dispersion from 25 to 65 °C the absorption band of PNA nucleobases increases in intensity. These findings could be explained by the existence, at room temperature, of some stacking interactions among the different PNA tetramers linked onto HNTs which are denatured into single-stranded state, at higher temperature. The different behavior between free PNA tetramers and the ones linked to HNTs could be explained by considering the presence of halloysite which gives rise to a more compact and ordered structure. By plotting the absorbance value at 260 nm *vs* the temperature, we calculate a melting temperature of ca. 40 °C, in agreement with the short chain length of the PNA tetramer.

The cooling of the HNTs-**7** dispersion did not lead to a rehybridization of the interaction since no variation in the absorbance values occurs (Figure S.5b).

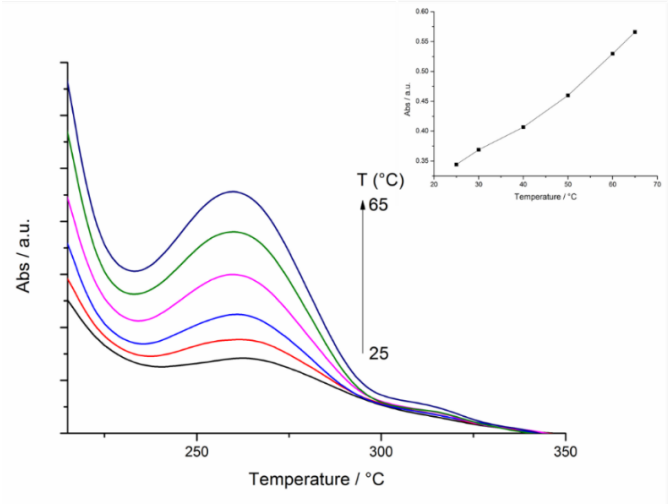

Figure 4. UV-*vis* spectra of aqueous dispersion of HNTs-**7** (0.06 mg mL^{-1}) nanomaterial recorded at different temperature; the insert shows the trend of the absorbance at 260 nm as a function of temperature.

Scanning Electron Microscopy (SEM) images showed that HNTs-**7** (Figure 5A), in contrast to pristine HNTs (Figure S.6),[31] displays a compact structure keeping HNTs glued together forming aggregates; where the tubular shape of halloysite is barely observable. The observed morphology could be reasonably ascribed to the Watson and Crick interactions caused by the PNA tetramers linked onto the HNTs external surface.

High Angle Annular Dark Field Scanning TEM (HAADF-STEM) imaging showed that the structure of HNTs (Figure 5B) was preserved after tetramer linkage. The HNTs-**7** nanomaterial exhibits the characteristic hollow tubular structure of halloysite as a shell with an organic core.

Energy Dispersive X-ray Spectroscopy (EDS) spectrum was also obtained by integration over the entire region and confirmed the presence of C and N atoms from the PNA tetramers linked onto HNTs-**7** nanomaterial besides the Al, Si and O atoms related to the inorganic support (Figure 5C). EDS elemental mapping showed that the PNA tetramers are localized at the external surface of HNTs wrapping the tubes (Figure 5D-F).

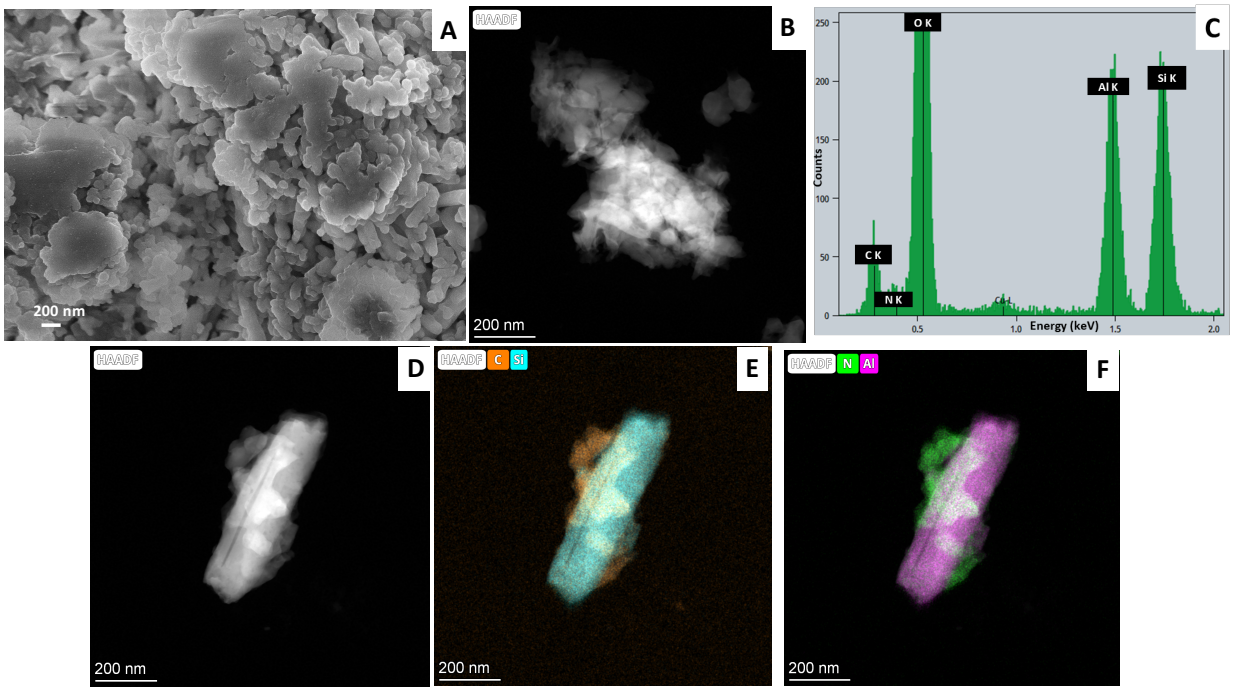

Figure 5. (a) SEM and (b) HAADF-STEM images of HNTs-**7** nanomaterial; (c) EDX spectrum; (d-e) EDX elemental mapping images.

Study on the interaction between HNTs-7 and ssDNA.

To investigate if the PNA tetramers retained its binding ability towards single-stranded DNA (ssDNA) when attached to the clay we performed some binding investigations.

We choose to investigate the interaction with single-stranded DNA instead of complementary single-strand RNA since DNA is more resistant against nucleases and does not require any chemical modification for handling that could alter its recognition properties.

Preliminary investigations about the interaction between the HNTs-**7** nanomaterial and the parallel and antiparallel ssDNA were performed by Isothermal Titration Calorimetry (ITC). Unfortunately, the net thermal effect could not provide evidence for the interaction between ssDNA and HNTs-**7**. It should be noted that HNTs dispersions, because of friction, generate a relatively high baseline signal that might disturb the small heat of interaction expected based on literature reports.[32] Based on these findings, we decided to study the interaction with Resonance Light Scattering (RLS) measurements.

RLS is a special elastic scattering technique that arises from the fluctuations of the solution refraction index; it allows the detection of the presence in solution of aggregates and has been extensively used for the study of aggregation processes of organic molecules or macromolecules.

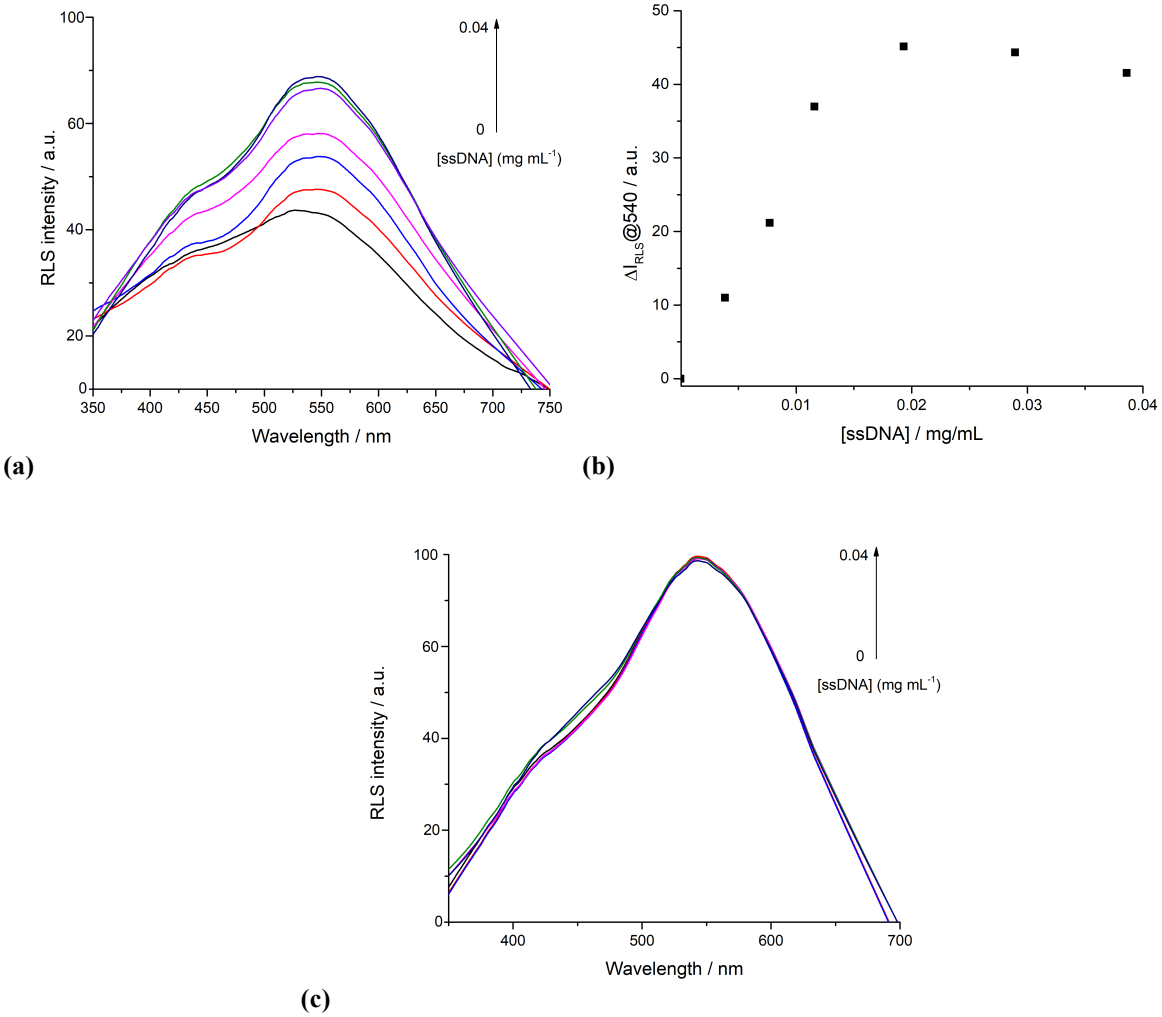

Figure 6. (a) RLS spectra of HNTs-**7** (0.1 mg mL^{-1}) and trend of RLS intensity as a function of (b) antiparallel ssDNA and (c) parallel ssDNA concentration (ranging from 0 to 0.04 mg mL^{-1}).

RLS experiments were performed by keeping HNTs-**7** concentration constant (0.1 mg mL^{-1}) and titrating with an increasing concentration of parallel or antiparallel ssDNA in the concentration range 0–0.04 mg mL^{-1} at 25 °C. By adding increasing concentrations of antiparallel ssDNA, we observed an increase in the RLS spectra of HNTs-**7** (Figure 6a). In Figure 6b are reported the trend of RLS at 540 nm as a function of antiparallel ssDNA concentration. As it is possible to observe, the RLS intensity increases with DNA concentration, indicating a binding between HNTs-**7** and the ssDNA and therefore the presence of nanoparticles with greater dimensions. Interestingly, a plateau was observed at DNA concentration of 0.02 mg mL^{-1} which corresponds to a stoichiometric ratio PNA/DNA of 1:1.

Conversely, by adding increasing concentration of parallel ssDNA we did not observe any change in the nanoparticle dimensions and therefore, in this case, no binding occurs (Figure 6c). The latter result confirmed the selectivity of the interaction between complementary antiparallel ssDNA and PNA, whereas no interaction occurs between ssDNA and HNTs surface.

In the light of higher binding affinity of RNA strands towards complementary PNAs,[33] in comparison to the DNA ones, we can assume that similar results could be obtained with ssRNA.

HNTs-8 *in vitro* experiments of cellular uptake

The cellular uptake of the obtained nanomaterial was investigated by CLSM experiments. To achieve this goal, the HNTs-**7** nanomaterial was labelled with a fluorescent coumarin chromophore combined with a switchable halochromic oxazine (**1Cl**) (Figure S.7).[34, 35] to obtain the fluorescent HNTs-**8** nanomaterial. The total amount of **1Cl** loaded onto HNTs-**7** nanomaterial was 1 wt%. The fluorescent probe **1Cl** was chosen since it shows an intense blue or red emission in the electromagnetic spectrum region after appropriate external stimuli. In addition, we previously demonstrated that it strong interacts with HNTs (HNTs/**1Cl**), and kinetic experiments showed that a negligible leaching of the probe from the clay occurred.[27] Furthermore, CLSM experiments showed that the HNTs/**1Cl** nanomaterial reached the intracellular compartments of the cells on a relatively short time scale (1 h), surrounding cell nuclei. Based on the above findings, the fluorescent HNTs-**8** nanomaterial could be considered stable and can be used in biological applications. Furthermore, due to the biocompatibility of the components constituting the HNTs-**8** nanomaterial,[27] it is a biocompatible nanomaterial as well, showing no *in vitro* cytotoxicity in all cell lines investigated at the experimental concentration used.

To explore the cellular uptake and distribution, HNTs-**8** was incubated (0.5 mg mL^{-1} up to 24 h) with three different living cell lines, namely hTERT (epithelial cells), MCF-7 (breast cancer) HL-60R (multidrug-resistant acute myeloid leukemia) chosen as models for normal cells, tumor cells growing adherent to the support, and floating tumor cells, respectively. Live cell images of HNTs-**8** are shown in Figure 7. We observed a very fast cellular uptake of HNTs-**8** in all three cell lines investigated with a high concentration of the nanomaterial localized inside the cells since 1 h of incubation, as highlighted by the intense fluorescent spots clearly observable in all cell lines.

Some punctate blue fluorescence is also observed, these foci are inside cells, as verified by the cross-sectional CLSM images. The appearance of punctuates near the nucleus and distributed throughout the cell suggested that the internalization could be a result of endocytosis, as predicted for HNTs-mediated cellular uptake.[27] When longer exposure times were used (6 and 24 h), fluorescence was localized within the cells and showed significant cytosolic distribution and lysosomal accumulation predominantly in the normal cell line hTERT with a point distribution that is indicative of compartmentalization. On the contrary, a diffuse fluorescence with a distribution at the boundary between the nucleus and the cytoplasm is observed in the tumor cell lines MCF-7 and HL-60R. Since the fluorescent probe can be detected by two different channels, the different fluorescence observed in the three cell lines could be attributable to the diverse nature of them.[36]

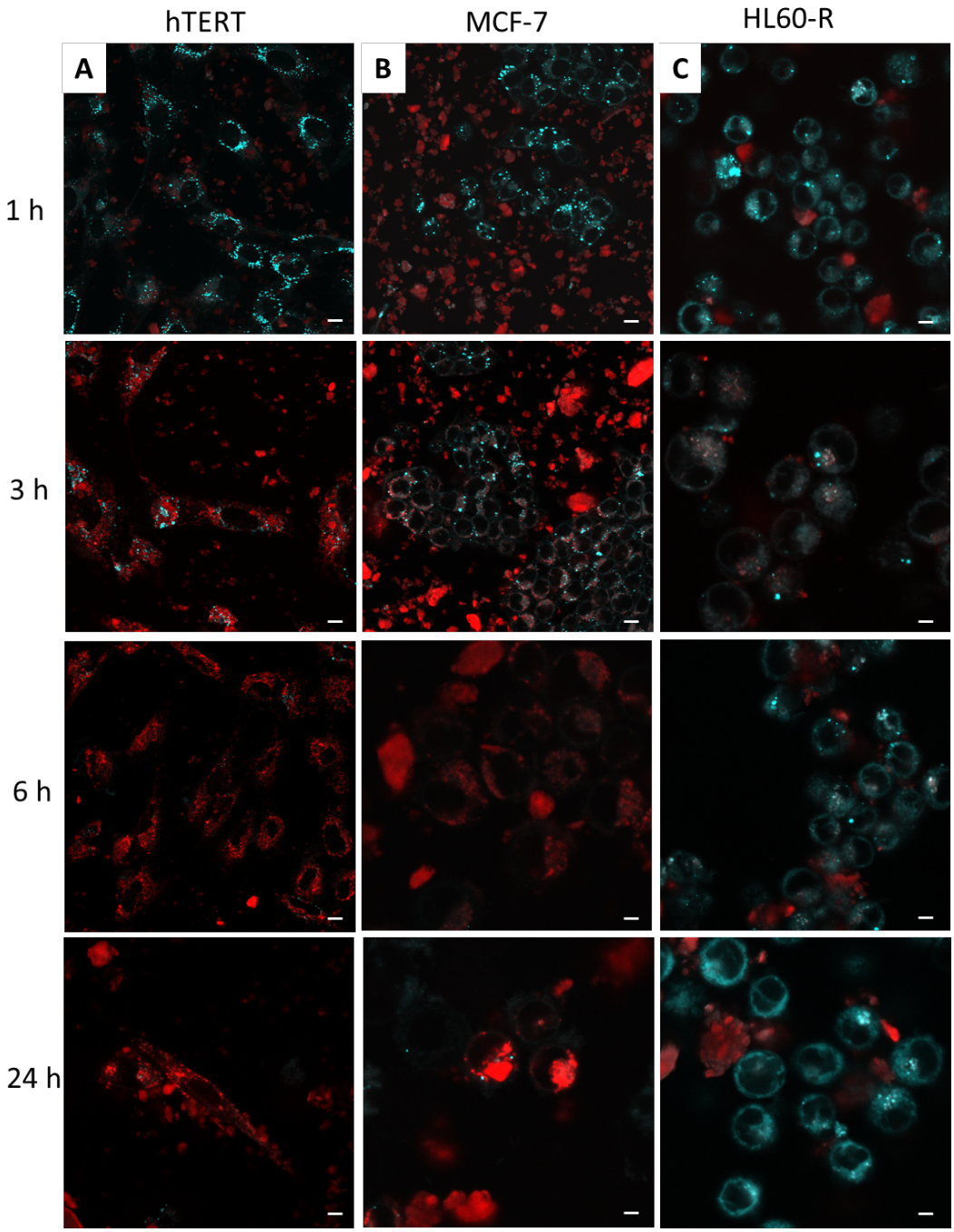

Figure 7. Merged CLSM images of hTERT, MCF-7 and HL60-R cell lines incubated with labeled HNTs-**8** at different times. Images were recorded under excitation at 405 and 595 nm. Scale bar 10 μm.

Kinetic release

Finally, in order to verify that after internalization the HNTs-**8** nanomaterial still retain PNA tetramers moieties linked to the carrier, kinetic release experiments of the PNA tetramer from HNTs-**7** nanomaterial was performed and the data analysed by UV-*vis* measurements. The kinetic release was carried out from HNTs-**7** in place of HNT-**8** to remove the adsorption bands in the UV-*vis* spectra

associated with **1Cl**. Kinetic release experiments were performed by the dialysis bag method, using conditions designed to mimic physiological conditions (phosphate buffers and HCl $1 \cdot 10^{-3}$ N at pH 7.4 and 3.0, respectively). The obtained kinetic data are shown in Figure 8. In neutral conditions, we observed a faster release of PNA_{ts} from HNTs-**7** nanomaterial with ca. 40 wt% of the total amount of PNA linked onto HNTs surface, released in 500 min, after which we observed a *plateau*. Different behavior was obtained in the case of acidic medium. We found that the PNA tetramers are almost quantitatively released within 24 h because of the hydrolysis of the imine bond that occurs in acidic medium.

These results confirmed that the HNTs-**7,** and consequentially HNTs-**8**, carrier can effectively deliver the PNA_{ts} inside the cells, promoting, therefore, its cellular uptake.

To better understand the release of PNA from halloysite carrier, the experimental data were analyzed by Power Fit and first-order models.

The results showed that at pH 7.4 the release of PNA_{ts} from HNTs-PNA nanomaterial follows the first order model (M_∞= 41 ± 6 wt%; k = 0.0051 ± 0.0006 min^{-1}, R^2=0.9805), indicating that after the slow cleavage of the imine bond, the diffusion of the molecule occurs through the dialysis membrane. Conversely, in acidic medium the release of PNA tetramer from HNTs-**7** follows a Power fit model (k = 1.33 ± 0.06 min^{-1}; n = 0.584 ± 0.008, R^2 = 0.9978). Since the n value is greater than 0.5, we assumed that the release of PNA tetramer is ruled by a non-Fickian mechanism.

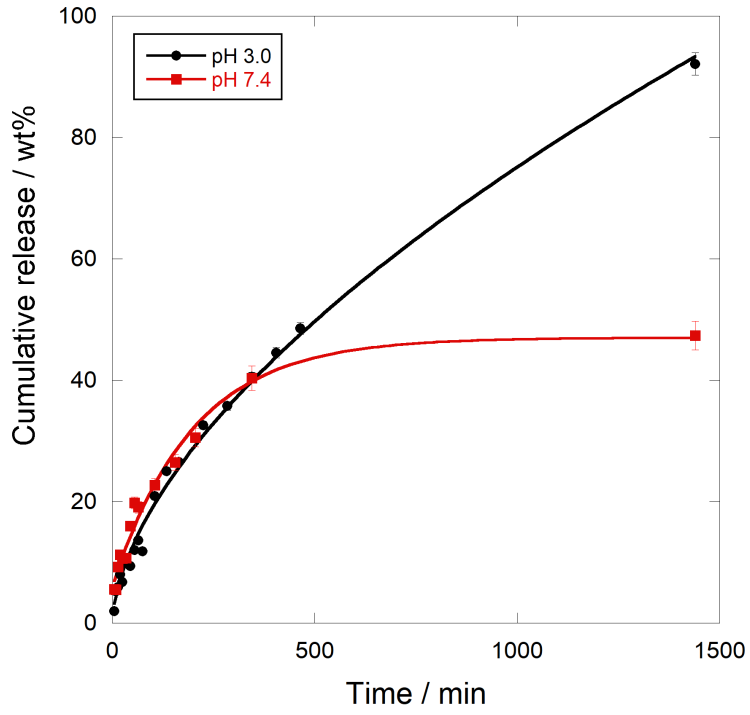

Figure 8. Kinetic release of PNA tetramer from HNTs-**7** in HCl $1 \cdot 10^{-3}$ M and phosphate buffer (0.05 M) solution at pH 7.4, at 37 °C. Reported are the mean ± standard deviation values of two independent experiments.

Conclusions

In the last years, the delivery of genetic material into a target site represents a challenge for modern medicine; in this context, HNTs have been considered smart delivery systems of biomedical interest. The development of single-strained PNA and synthetic DNA/RNA mimics, has attracted attention as promising therapeutic molecules for diagnostic and gene therapy. However, PNA possess some limitations such as scarce cell uptake and poor water solubility which limited their practical applications. To solve these problems, PNAs need to be delivered by carrier systems. Although some inorganic systems, such as zeolite and silica, have been used for the delivery of PNA [37], up to now no studies deal with the development of halloysite based carrier systems and more important the PNA covalent linkage onto carrier surface.

In this study, we disclosed a synthetic strategy to covalent link a single-strained PNA tetramer (chosen as model) on HNTs external surface in order to obtain an antisense agent based on HNTs-PNA nanomaterial.

The covalent modification of HNTs external surface with the PNA tetramer, was explored by a pH sensitive imine bond. Several synthetic approaches for the linkage between HNTs and PNA_{ts} were explored, and the successful modification was confirmed by TGA, DSC, FT-IR and UV-*vis* spectroscopies. The morphology of obtained nanomaterial was studied by SEM and HAADF/STEM coupled with EDX and its aqueous mobility was investigated by DLS and ζ–potential measurements. Furthermore, the ability of the obtained nanomaterial to bind complementary single-stranded DNA (ssDNA) was assessed by RLS measurements. In addition, after the nanomaterial labelling with the fluorescent probe **1Cl**, its cellular uptake was evaluated by confocal laser-scanning microscopy (CLSM) measurements on normal (hTERT) and tumoral cell lines (MCF-7 and HL-60R). Finally, to demonstrate that after internalization of the nanomaterial the PNA tetramers are still covalently bound to the clay, the pH-sensitive nature of the covalent bond between HNTs and PNA derivatives by kinetic release experiments at different pH conditions (pH 3.0 and 7.4, respectively) was esteemed.

In conclusion, herein we used, for the first time, HNTs as carriers for PNA delivery into three different cell lines. We found that the binding ability of PNA towards complementary single-stranded DNA remains intact even after its covalent linkage on HNTs external surface. Compared to others inorganic nanocarriers, commonly used for PNA delivery, HNTs, natural aluminosilicate clay with hollow tubular structure, available in large amount at low cost, could offer the advantage to simultaneous co-delivery different active species by the selectively modification of surfaces both by covalent or supramolecular interactions. In addition, HNTs can efficiently transport PNA inside cells, localizing

themselves in the perinuclear region. Furthermore, the covalent linkage of PNA onto HNTs surface ensures a targeted release in acidic environment.

The obtained results do the groundwork for future developments of halloysite carriers for specific PNA sequences for the treatment of several diseases. To the light of the no-biodegradability of HNTs, it is possible to hypothesize a future use of the developed systems for oral, topical or local administration.

Materials and Methods

The monomers Boc-PNA-**T**-OH (> 95%), Boc-PNA-**C**(Cbz)-OH (> 95%), Boc-PNA-**G**(Cbz)-OH (> 95%), Boc-PNA-**A**(Cbz)-OH (> 95%) purchased from ASM Research Chemicals GmbH (Hannover, Germany), the 4-azidocinnamaldehyde (> 98%) was purchased from TCI Chemical, HNTs (lyophilized powder, MQ200) were purchased from Merck (Darmstadt, Germany). The polystyrene resin MBHA (loading of 0.74 mmol/g) was purchased from Merck (Darmstadt, Germany), and it was downloaded to 0.2 mmoL g^{-1} with the Boc-thymine PNA monomer. Polypropylene one-way syringes and the corresponding polytetrafluoroethylene (PTFE) frits, used as reactor for the manual solid phase synthesis, were purchased from Alltech Associates Inc. (Lokeren, Belgium). Parallel and antiparallel ssDNA were purchased from Eurofins Genomics.

Resin supported PNA tetramer **1** and HNTs–$\mathbf{NH_2}$ were synthetized as reported elsewhere.[28, 29]

The reverse-phase RP-HPLC analyses were performed on Agilent technologies 1200 Series system, using the analytical column Luna C18 (25 cm × 4.6 mm, 5 μm) at a flow rate of 1 mL/min. Solvent A (0.1% TFA in water) and solvent B (0.1% TFA in acetonitrile) were used at specific gradients based on the polarity of the products, with detection by UV at 260 nm.

ESI mass analyses were recorded by mass spectrometer Thermo Scientific LCQ Fleet for ESI analysis, dissolving the sample in a suitable solvent.

FT-IR spectra (KBr) were acquired with an Agilent Technologies Cary 630 FT-IR spectrometer.

UV–*vis* measurements were performed using a Beckmann DU 650 spectrometer.

The thermogravimetric analysis (TGA) of the material was performed in a TGA/DSC1 STAR System from Mettler Toledo Inc. The sample (15 mg) was subjected to a pre-treatment in air flow (30 mL/min) from 25 °C to 100 °C with a heating rate of 10 °C/min and holding time at 100 °C for 30 min, in order to remove any eventual physisorbed water. Then, the temperature was increased from 100 to 1000 °C under air flow (30 mL/min) and the weight loss occurring during this step was considered in order to calculate the organic weight content of the HNTs based nanomaterial.

The size analysis, ζ–potential and polydispersity index of the samples were determined using a Malvern Zetasizer Nano ZS instrument, fitted with a 532-nm laser at a fixed scattering angle of 173°.

DSC measurements were carried out on a DSC Q200 calorimeter interfaced to a TA Thermal Analyst 3100 controller connected to an RCS90 cooling system. Heating cycles were done in a 50 mL/min stream of nitrogen. Samples were weighed in T-zero aluminum pans. For each sample, after equilibration of the sample at 25 °C, DSC measurements were performed using a temperature ramp with a rate of 10 °C/min from 30 °C to 150 °C.

RLS measurements were performed at 25 °C on a spectrofluorophotometer (Jasco FP-777 W) equipped with a system for temperature control. A synchronous scanning mode was used, and monochromators of emission and excitation were preset to identical wavelengths. The RLS spectrum was recorded from 200 to 750 nm with both the excitation and emission slit widths set at 1.5 nm.

Transmission electron microscopy (TEM) was performed by means of a FEI Titan G2 60–300 ultra-high-resolution transmission electron microscope (FEI, Lausanne, Switzerland) coupled with analytical electron microscopy (AEM) performed with a SUPER X silicon drift windowless energy dispersive X-ray spectroscopy (XEDS) detector. AEM spectra were saved in mode STEM (scanning transmission electron microscopy) with a HAADF (high angle annular dark field) detector.

Scanning electron microscopy (SEM) images were acquired with a GEMINI (FESEM) CARL Zeiss coupled to an EDX microanalyser (Oxford Instruments). Samples were dried at 40 °C for a minimum of 48 h. Then, powdery samples were mounted over standard aluminum stubs and coated with carbon. Textural microphotographs were obtained at 3 kV, while EDX were acquired at 15 kV. In both cases, immersion lens detector was used (InLens, Zeiss).

ITC experiments were performed by using the ultrasensitive nano-ITC200 calorimeter (MicroCal). An amount of approximately 40 μL of the water/DNA mixture was injected into the thermally equilibrated ITC cell (200 μL) containing the water/HNTs-PNA dispersion (concentration of 0.19 mg mL^{-1}). Each addition step was 2 μL. Volumes have been calibrated by NaCl dilution experiment. The cell was thermally equilibrated at 25.000 ± 0.005 °C. The raw data were compared with the dilution experiments for an appropriate baseline subtraction.

Confocal images were acquired with an Olympus FluoView10i confocal laser scanning microscope (Olympus, Japan) equipped with humidity control and CO_2 using a 10 × 0.3 NA objective. The hTERT RPE-1-immortalized retinal pigment epithelial cell line and MCF-7 breast cancer cell line used in this study were cultured in DMEM medium supplemented with 1% glutamine, 10% heat-inactivated fetal bovine serum and 100 U/mL penicillin and 100 μg/mL streptomycin, HL-60R drug resistant acute myeloid leukemia cells were cultured in RPMI medium supplemented with 1% glutamine, 10% heat-inactivated fetal bovine serum and 100 U/mL penicillin and 100 μg/mL streptomycin in a humidified 5% CO_2 atmosphere at 37 °C. Cells were seeded on chamber slide system at a density of 10.000 cells/well containing 300 μL of complete medium and incubated

overnight at 37 °C in a humidified 5% CO_2 atmosphere. After 24 h, the medium was replaced with a fresh complete medium and the cells were treated with an aliquot of HNTs-**8** dispersed in water. Measurement was acquired using laser excitation at 405 nm or 595 nm. Emitted fluorescence was acquired in photon-counting mode. Spectral detection has been performed using a bandwidth of 5 nm and a step size of 3 nm in the range 420–740 nm. The scan area was 256 × 256 pixels and the scan speed were 12 µs per pixel.

Synthesis of compound 4

To a solution of succinic anhydride (250 mg, 2.5 mol, 1.14 eq) and DMAP (253 mg, 2.1 mmol, 0.95 eq) in DCM (6 mL), propargylamine (141 µL, 121.3 mg, 2.2 mmol, 1 eq) was added, and the resulting mixture was stirred at room temperature for 1 h. Then the solution was washed with a 5% aqueous solution of Na_2CO_3 (6 mL) to achieve a basic pH. The aqueous phase was collected and acidified with 10 mL of HCl 1 M, checking the pH was acid. The acidic aqueous phase was extracted with ethyl acetate (6 × 5mL), and the collected organic phases were dried with Na_2SO_4, filtered and the solvent was removed under vacuum. The crude product **4** (170 mg, 1.1 mmol, yield 50%) was obtained as a colorless solid, and it was used in the following reaction without further purification.

^{1}H-NMR (300 MHz, CD_3OD), δ (ppm): 2.49 (t, 2H, CH_2), 2.60 (t, 2H, CH_2), 3.32 (t, 1H, CH), 3.95 (d, 2H, CH_2), 4.87 (s, 1H, OH)

Synthesis of compound 3

The resin supported PNA tetramer **1** (330 mg, 0.066 mmol, 1 eq) was first swollen with DCM (4 mL) for 2 h, treated with a TFA/*m* cresol (95:5) solution (2 × 3 mL, 4 min), and then washed with DCM (3 × 3 mL) and NMP (3 × 3 mL). In a vial, a solution of DIPEA (115 µL, 85.3 mg, 0.66 mmol, 10 eq) and intermediate **4** (48 mg, 0.31 mmol, 5.3 eq) in NMP (ca. 2 mL) was added to a solution of HATU (120 mg, 0.32 mmol, 4.8 eq 4.8 eq) in NMP, and the resulting mixture was shaken for 2 min. The activated mixture was then added to the resin and shaken at room temperature for 4 h. The resin was washed with NMP (3 × 5 mL) and DCM (3 × 5 mL). The resin was finally washed with TFA, and subsequently stirred for 1 h with a mixture of TFA/TFMSA/thioanisole/*m*-cresol in a 6:2:1:1 ratio. The reaction mixture was filtered, and the resin washed with TFA. The filtrate was concentrated, and Et_2O was added to precipitate PNA tetramer as a white solid. Centrifugation of the slurry gave the product, which was washed with Et_2O and dried to afford the crude modified PNA tetramer **3**, that was analyzed by mass analysis and HPLC.

MW= 1238.2 g/mol

RP-HPLC (from H_2O/TFA 0.1% CH_3CN/TFA 0.1% 95:5 to H_2O/TFA 0.1% CH_3CN/TFA 0.1% 0:100 in 50 min), rt (min): 8.4

ESI(+)-MS, m/z: 1239 (M+1)

Synthesis of HNTs-6

In a 25 mL round bottom flask were introduced 200 mg of HNTs-**NH_2**, 515 mg of 4-azidocinnamaldehyde (2.97 mmol) and 10 mL of EtOH. The obtained dispersion was left to stir at reflux for 24 h. Then the solid was washed several times with ethanol and dried at 60 °C overnight.

Synthesis of HNTs-7

In a 10 mL round bottom flask were introduced 50 mg of HNTs-**6**, 37 mg of compound **3** (0.03 mmol) and 2 mL of a mixture of H_2O/^{t}BuOH (1:1). To the obtained dispersion were added 0.050 mL of a $CuSO_4$ aqueous solution (1 M) and 0.500 mL of an aqueous solution of sodium ascorbate (1 M). The mixture was left to stir at room temperature for ca. 24 h. Then the solid was washed several times with water and dried at 60 °C overnight.

Kinetic Release

The release of PNA tetramer moieties from HNTs-**7** was done as follows: 20 mg of the sample were dispersed in 1 mL of dissolution medium (phosphate buffers and HCl $1 \cdot 10^{-3}$ N at pH 3.0 and 7.4, respectively) and transferred into a sealed dialysis membrane (Medicell International Ltd MWCO 12-14000 with a diameter of 21.5 mm). Subsequently the membrane was put in a round bottom flask containing 9 mL of the release medium at 37 °C and stirred. At fixed time, 1 mL of the release medium has been withdrawn and analysed by UV-*vis* measurements at λ of 315 nm (maximum absorption band of 4-azido cinnamaldehyde, to avoid interferences due to the absorption of buffer solution in the same absorption range of PNA). To ensure sink conditions, 1 mL of fresh solution has been used to replace the collected one. Total amounts of drug released (F_t) were calculated as follows:

$$F_t = V_m C_t + \sum_{i=0}^{t-1} V_a C_i \qquad \text{(Eq. 1)}$$

where V_m and C_t are the volume and the concentration of the drug at time t. V_a is the volume of the sample withdrawn and C_i is the drug concentration at time i ($i < t$).

CREDIT AUTHORS STATEMENT

Massaro, M. Formal analysis, investigation, writing – original draft, , writing – review & editing

Cauteruccio, S. Formal analysis, investigation

Lazzara, G. Formal analysis, investigation

Liotta, L.F. Formal analysis, investigation

Licandro, E. Conceptualization, methodology, project administration, supervision, writing – original draft

Notarbartolo, M. Formal analysis, investigation

Raymo, F. Formal analysis, investigation

Sánchez-Espejo, R. Formal analysis, investigation

Viséras-Iborra, C. Formal analysis, investigation

Riela, S. Conceptualization, methodology, project administration, supervision, writing – review & editing.

ACKNOWLEDGMENTS

The work was carried out in the frame of the PON "AIM: Attrazione e Mobilità Internazionale" No. 1808223-1 project. Confocal, DLS and ζ-potential measurements were performed at ATeN Center – University of Palermo.

References

[1] F. Pellestor, P. Paulasova, The peptide nucleic acids (PNAs), powerful tools for molecular genetics and cytogenetics, European Journal of Human Genetics 12(9) (2004) 694-700.
[2] P.E. Nielsen, M. Egholm, R.H. Berg, O. Buchardt, Sequence-Selective Recognition of DNA by Strand Displacement with a Thymine-Substituted Polyamide, Science 254(5037) (1991) 1497-1500.
[3] M. Egholm, O. Buchardt, L. Christensen, C. Behrens, S.M. Freier, D.A. Driver, R.H. Berg, S.K. Kim, B. Norden, P.E. Nielsen, PNA hybridizes to complementary oligonucleotides obeying the Watson–Crick hydrogen-bonding rules, Nature 365(6446) (1993) 566-568.
[4] P.E. Nielsen, Structural and biological properties of peptide nucleic acid (PNA), Pure and Applied Chemistry 70(1) (1998) 105-110.
[5] V.V. Demidov, V.N. Potaman, M.D. Frank-Kamenetskil, M. Egholm, O. Buchard, S.H. Sönnichsen, P.E. Nlelsen, Stability of peptide nucleic acids in human serum and cellular extracts, Biochemical Pharmacology 48(6) (1994) 1310-1313.
[6] V.L. Marin, S. Roy, B.A. Armitage, Recent advances in the development of peptide nucleic acid as a gene-targeted drug, Expert Opinion on Biological Therapy 4(3) (2004) 337-348.
[7] A. Gupta, A. Mishra, N. Puri, Peptide nucleic acids: Advanced tools for biomedical applications, Journal of Biotechnology 259 (2017) 148-159.
[8] C. Sharma, S.K. Awasthi, Versatility of peptide nucleic acids (PNAs): role in chemical biology, drug discovery, and origins of life, Chemical Biology & Drug Design 89(1) (2017) 16-37.
[9] A.P. Falanga, V. Cerullo, M. Marzano, S. Feola, G. Oliviero, G. Piccialli, N. Borbone, Peptide Nucleic Acid-Functionalized Adenoviral Vectors Targeting G-Quadruplexes in the P1 Promoter of Bcl-2 Proto-Oncogene: A New Tool for Gene Modulation in Anticancer Therapy, Bioconjugate Chemistry 30(3) (2019) 572-582.
[10] F. Amato, R. Tomaiuolo, F. Nici, N. Borbone, A. Elce, B. Catalanotti, S. D'Errico, C.M. Morgillo, G. De Rosa, L. Mayol, G. Piccialli, G. Oliviero, G. Castaldo, Exploitation of a Very Small Peptide Nucleic Acid as a New Inhibitor of miR-509-3p Involved in the Regulation of Cystic Fibrosis Disease-Gene Expression, BioMed Research International 2014 (2014) 610718.
[11] P.E. Nielsen, Addressing the challenges of cellular delivery and bioavailability of peptide nucleic acids (PNA), Quarterly Reviews of Biophysics 38(4) (2006) 345-350.
[12] G. Chen, Y. Qian, H. Zhang, A. Ullah, X. He, Z. Zhou, H. Fenniri, J. Shen, Advances in cancer theranostics using organic-inorganic hybrid nanotechnology, Applied Materials Today 23 (2021) 101003.
[13] A. Bertucci, E.A. Prasetyanto, D. Septiadi, A. Manicardi, E. Brognara, R. Gambari, R. Corradini, L. De Cola, Combined Delivery of Temozolomide and Anti-miR221 PNA Using Mesoporous Silica Nanoparticles Induces Apoptosis in Resistant Glioma Cells, Small 11(42) (2015) 5687-5695.
[14] K.R. Beavers, J.W. Mares, C.M. Swartz, Y. Zhao, S.M. Weiss, C.L. Duvall, In Situ Synthesis of Peptide Nucleic Acids in Porous Silicon for Drug Delivery and Biosensing, Bioconjugate Chemistry 25(7) (2014) 1192-1197.
[15] D. Peixoto, I. Pereira, M. Pereira-Silva, F. Veiga, M.R. Hamblin, Y. Lvov, M. Liu, A.C. Paiva-Santos, Emerging role of nanoclays in cancer research, diagnosis, and therapy, Coordination Chemistry Reviews 440 (2021).

[16] E. Tarasova, E. Naumenko, E. Rozhina, F. Akhatova, R. Fakhrullin, Cytocompatibility and uptake of polycations-modified halloysite clay nanotubes, Applied Clay Science 169 (2019) 21-30.
[17] A. Stavitskaya, G. Fakhrullina, L. Nigamatzyanova, E. Sitmukhanova, E. Khusnetdenova, R. Fakhrullin, V. Vinokurov, Biodistribution of quantum dots-labelled halloysite nanotubes: A caenorhabditis elegans in vivo study, Materials 14(19) (2021).
[18] S. Riela, A. Barattucci, D. Barreca, S. Campagna, G. Cavallaro, G. Lazzara, M. Massaro, G. Pizzolanti, T.M.G. Salerno, P. Bonaccorsi, F. Puntoriero, Boosting the properties of a fluorescent dye by encapsulation into halloysite nanotubes, Dyes and Pigments 187 (2021).
[19] M.V. Gorbachevskii, A.V. Stavitskaya, A.A. Novikov, R.F. Fakhrullin, E.V. Rozhina, E.A. Naumenko, V.A. Vinokurov, Fluorescent gold nanoclusters stabilized on halloysite nanotubes: in vitro study on cytotoxicity, Applied Clay Science 207 (2021).
[20] M. Massaro, G. Barone, G. Biddeci, G. Cavallaro, F. Di Blasi, G. Lazzara, G. Nicotra, C. Spinella, G. Spinelli, S. Riela, Halloysite nanotubes-carbon dots hybrids multifunctional nanocarrier with positive cell target ability as a potential non-viral vector for oral gene therapy, Journal of Colloid and Interface Science 552 (2019) 236-246.
[21] M. Massaro, P. Poma, G. Cavallaro, F. García-Villén, G. Lazzara, M. Notarbartolo, N. Muratore, R. Sánchez-Espejo, C. Viseras Iborra, S. Riela, Prodrug based on halloysite delivery systems to improve the antitumor ability of methotrexate in leukemia cell lines, Colloids and Surfaces B: Biointerfaces 213 (2022).
[22] F.R. Ahmed, M.H. Shoaib, M. Azhar, S.H. Um, R.I. Yousuf, S. Hashmi, A. Dar, In-vitro assessment of cytotoxicity of halloysite nanotubes against HepG2, HCT116 and human peripheral blood lymphocytes, Colloids and Surfaces B: Biointerfaces 135 (2015) 50-55.
[23] X. Wang, J. Gong, Z. Gui, T. Hu, X. Xu, Halloysite nanotubes-induced Al accumulation and oxidative damage in liver of mice after 30-day repeated oral administration, Environmental Toxicology 33(6) (2018) 623-630.
[24] Z. Long, Y.P. Wu, H.Y. Gao, Y.F. Li, R.R. He, M. Liu, Functionalization of Halloysite Nanotubes via Grafting of Dendrimer for Efficient Intracellular Delivery of siRNA, Bioconjugate Chemistry 29(8) (2018) 2606-2618.
[25] Z. Long, J. Zhang, Y. Shen, C. Zhou, M. Liu, Polyethyleneimine grafted short halloysite nanotubes for gene delivery, Materials Science and Engineering C 81 (2017) 224-235.
[26] S. Batasheva, M. Kryuchkova, R. Fakhrullin, G. Cavallaro, G. Lazzara, F. Akhatova, L. Nigamatzyanova, V. Evtugyn, E. Rozhina, R. Fakhrullin, Facile Fabrication of Natural Polyelectrolyte-Nanoclay Composites: Halloysite Nanotubes, Nucleotides and DNA Study, Molecules 25(15) (2020).
[27] M. Massaro, M. Notarbartolo, F.M. Raymo, G. Cavallaro, G. Lazzara, M.M.A. Mazza, C. Viseras-Iborra, S. Riela, Supramolecular Association of Halochromic Switches and Halloysite Nanotubes in Fluorescent Nanoprobes for Tumor Detection, ACS Applied Nano Materials (2022).
[28] G. Prencipe, S. Maiorana, P. Verderio, M. Colombo, P. Fermo, E. Caneva, D. Prosperi, E. Licandro, Magnetic peptide nucleic acids for DNA targeting, Chemical Communications (40) (2009) 6017-6019.
[29] M. Massaro, A. Borrego-Sánchez, R. Sánchez-Espejo, C. Viseras Iborra, G. Cavallaro, F. García-Villén, S. Guernelli, G. Lazzara, D. Miele, C.I. Sainz-Díaz, G. Sandri, S. Riela, Ciprofloxacin carrier systems based on hectorite/halloysite hybrid hydrogels for potential wound healing applications, Applied Clay Science 215 (2021).
[30] M. Massaro, R. Amorati, G. Cavallaro, S. Guernelli, G. Lazzara, S. Milioto, R. Noto, P. Poma, S. Riela, Direct chemical grafted curcumin on halloysite nanotubes as dual-responsive prodrug for pharmacological applications, Colloids and Surfaces B: Biointerfaces 140 (2016) 505-513.
[31] M. Massaro, G. Barone, V. Barra, P. Cancemi, A. Di Leonardo, G. Grossi, F. Lo Celso, S. Schenone, C. Viseras Iborra, S. Riela, Pyrazole[3,4-d]pyrimidine derivatives loaded into halloysite as potential CDK inhibitors, International Journal of Pharmaceutics 599 (2021) 120281.

[32] A. Gourishankar, S. Shukla, K.N. Ganesh, M. Sastry, Isothermal Titration Calorimetry Studies on the Binding of DNA Bases and PNA Base Monomers to Gold Nanoparticles, Journal of the American Chemical Society 126(41) (2004) 13186-13187.
[33] K.K. Jensen, H. Ørum, P.E. Nielsen, B. Nordén, Kinetics for Hybridization of Peptide Nucleic Acids (PNA) with DNA and RNA Studied with the BIAcore Technique, Biochemistry 36(16) (1997) 5072-5077.
[34] E. Deniz, S. Sortino, F.M. Raymo, Fluorescence Switching with a Photochromic Auxochrome, J. Phys. Chem. Lett. 1(24) (2010) 3506-3509.
[35] E. Deniz, M. Tomasulo, J. Cusido, I. Yildiz, M. Petriella, M.L. Bossi, S. Sortino, F.M. Raymo, Photoactivatable Fluorophores for Super-Resolution Imaging Based on Oxazine Auxochromes, J. Phys. Chem. C 116(10) (2012) 6058-6068.
[36] Y. Gong, M. Duvvuri, J.P. Krise, Separate Roles for the Golgi Apparatus and Lysosomes in the Sequestration of Drugs in the Multidrug-resistant Human Leukemic Cell Line HL-60*, Journal of Biological Chemistry 278(50) (2003) 50234-50239.
[37] S. Volpi, U. Cancelli, M. Neri, R. Corradini, Multifunctional Delivery Systems for Peptide Nucleic Acids, Pharmaceuticals 14(1) (2021) 14.